JMEPEG (2011) 20:1357–1363
DOI: 10.1007/s11665-011-9897-0

1059-9495/$19.00

Room Temperature Ductility and Microstructure of Magnesium AZ31B Sheet

M.P. Miles, D. Fullwood, B.L. Adams, A. Khosravani, J. Scott, and R.K. Mishra

(Submitted November 13, 2010; in revised form January 26, 2011)

Formability of wrought magnesium alloys at room temperature or slightly elevated temperatures is modest, reaching about 20% elongation in a tension test and exhibiting poor resistance to strain localization and failure. The hexagonal close packed structure of Mg has few active slip systems at lower forming temperatures, limiting ductility and reducing applications in auto body structures. Much greater levels of ductility can be reached at higher temperatures (typically >300 °C), but this is expensive and inconvenient for a high-volume production environment. Tension testing and biaxial forming of annealed AZ31B magnesium alloy sheets were done at room temperature to various levels of strain. High-resolution electron back scatter diffraction (EBSD) was used to measure twin fraction and dislocation density, in order to find relationships between strain and potential failure locations within the microstructure. Twin fractions were found to have a weak positive correlation to uniaxial and biaxial tensile strain, while dislocation density was found to correlate more strongly with uniaxial tensile strain.

Keywords AZ31B, crack detection, dislocation density, high-resolution EBSD, magnesium, twinning

1. Introduction

The use of magnesium alloys in the automotive industry has increased in recent years as part of a large effort to reduce vehicle weight and to increase fuel economy (Ref 1-4). The potential weight savings for each part can be as high as 62% for the most stringent equivalent designs, when replacing steel parts. The bulk of magnesium parts in automotive applications are die cast, allowing for production of complex shapes. During the past 10-15 years, many efforts have been made to improve mechanical properties by reducing casting defects (Ref 5, 6). Despite these efforts an average vehicle still only contains 10-12 lbs of magnesium alloy compared to 300-400 lbs of other lightweight materials, such as aluminum and polymer composites. Die cast parts can be used in some applications, but their use is constrained by their modest mechanical properties (Ref 6, 7).

On the other hand, wrought magnesium alloys have better mechanical properties than cast alloys, increasing potential weight savings up to 78%, but ductility of wrought magnesium is limited to about 20% elongation at room temperature in a tension test while exhibiting poor resistance to strain localization. The reason for this is its hexagonal close packed structure, which typically favors slip on only two independent active slip systems on the basal plane (0001) and to deformation by twinning at room temperature (Ref 6-9). At this level of ductility it is not possible to form many parts with enough complexity to be useful, which significantly reduces possible applications for vehicle weight reduction. Therefore, one of the barriers to greater use of magnesium alloys in automotive structures is poor ductility at room temperature. Current practice requires a typical forming temperature of 300 °C or greater in order to achieve sufficient ductility for making complex shapes, thus adding cost to the manufacturing process (Ref 4, 10).

The focus of the current work is on magnesium alloy ductility at room temperature. A new technology, which we will call defect detection microscopy (DDM), is being developed in order to detect defect sites, or microstructural features like twins which may be a precursor to failure, in deformed polycrystalline materials. This technology will be used to study the microstructure in strained AZ31B samples to determine how strain path during room temperature forming affects material ductility. For example, twin density and dislocation density at different levels of deformation will be measured in strained specimens. Results are presented and discussed for AZ31B samples deformed in uniaxial and biaxial tension.

2. Experimental Procedures

AZ31B sheet with 1.8 mm thickness was obtained in the H24 condition and subsequently annealed at 350 °C for 15 min prior to the forming experiments. Tension testing was done on annealed specimens to various levels of strain, using the ASTM E8 standard, where both the rolling and transverse directions (RD and TD) of the sheet were oriented along the major strain axis. Uniaxial true tensile strains of 4, 8, and 12% were achieved. Samples were cut from each specimen for mounting and polishing in preparation for electron back scatter diffraction (EBSD) analysis. Scans were done on material taken from the

M.P. Miles, Manufacturing Engineering Technology, Brigham Young University, Provo, UT 84602; **D. Fullwood, B.L. Adams, A. Khosravani,** and **J. Scott**, Mechanical Engineering, Brigham Young University, Provo, UT 84602; and **R.K. Mishra**, General Motors R&D Center, Warren, MI 48090. Contact e-mail: mmiles@byu.edu.

center of the cross section in the middle of the gage length for both RD and TD specimens, at the midplane of the thickness, as shown in Fig. 1.

In addition to tension testing, biaxial stretch forming was done using limiting dome height (LDH) tooling, where polyethylene sheet coated in mineral oil was placed between the punch and the sheet in order to minimize friction. The dies which clamp the specimen were modified from the original LDH design, because the AZ31B sheet was not ductile enough to sustain clamping without fracture using a standard lockbead designed for mild steel. Modification of the clamping dies, where the lockbead design was adapted to AZ31B sheet, is shown in Fig. 2.

By using three smaller beads as seen in Fig. 2(b), the sheet was securely clamped without causing fracture in the specimen. Surface strain measurements were done using a 2 mm square grid checkerboard pattern which was applied to the sheet prior to forming, as shown in Fig. 3.

Surface strains were determined with the aid of a RAM optical image measurement machine, where undeformed and deformed grid patterns were compared in order to calculate changes in the grid dimensions. The changes in dimension were then employed to calculate true surface strains. After forming experiments were completed and strain levels were measured, samples were cut from the top of the dome, with the surface of interest for EBSD analysis oriented both parallel and perpendicular to the RD. The EBSD scans were done at the midplane of the sheet thickness on the samples cut from the dome.

The uniaxial tension and biaxial tension specimens were mechanically polished with sand paper, up to 1200 grit, and subsequently polished using oil-based diamond suspensions of 6, 3, and 1 μm. Final polishing was done using 0.02 μm colloidal silica, followed immediately by a rinse under running water. Finally, samples were etched with a solution of 60 mL ethanol, 20 mL distilled water, 15 mL acetic acid, and 5 mL nitric acid. Scans were performed using an EBSD camera attached to a FEI Helios Nanolab 600i at a voltage of 25 kV, with a square grid pattern of 200 × 200 μm and a step size of 50 nm.

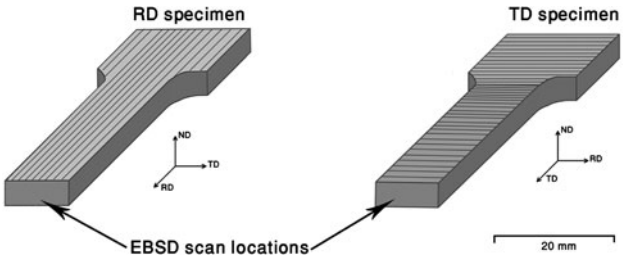

Fig. 1 Location of EBSD scans on RD and TD uniaxial tensile specimens

3. Defect Detection by Analysis of EBSD Scans

3.1 Calculation of Twin Fraction

Texture of the annealed and strained AZ31B sheets was obtained from the EBSD scans using the TSL™ OIM software (Ref 11). In addition to determining the textures, twin fractions were calculated for the annealed and the strained specimens. This was done by using scan data to identify boundaries with misorientations characteristic of twin boundaries in magnesium alloys, which is 86° for tension twins and 56° for compression twins, using a tolerance of plus or minus 2°. In addition to using misorientation across the boundary as a criterion for a twin plane, it is also necessary to verify that the plane of the boundary is one which corresponds to a twin plane. While EBSD scans are two dimensional in nature, the TSL™ software performs a check that the trace of the boundary plane is aligned

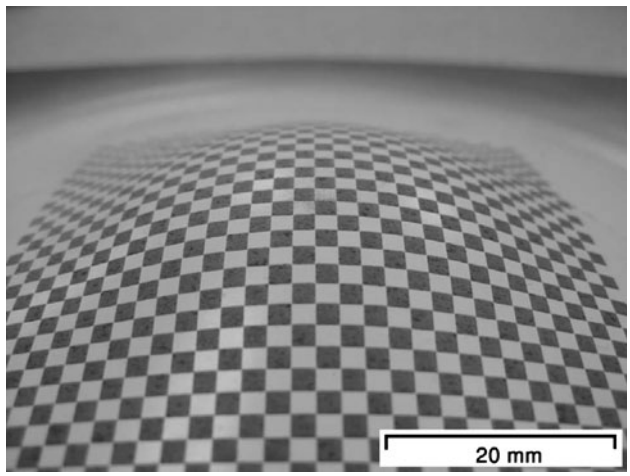

Fig. 3 Square grid pattern used for surface strain measurements

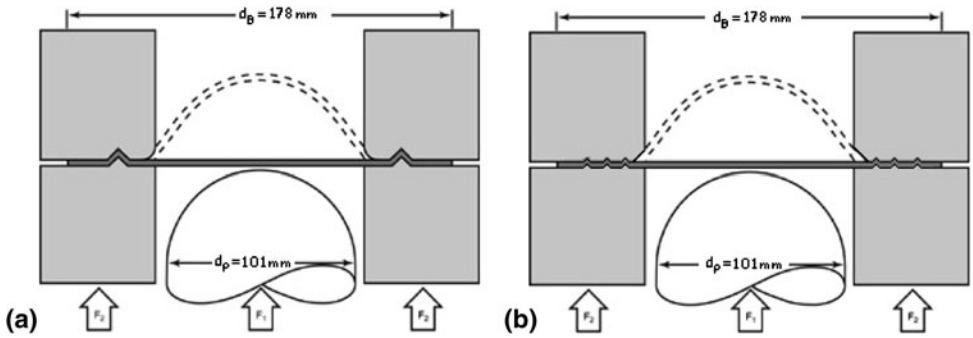

Fig. 2 Schematics showing LDH punch and dies. The standard clamping dies with one large lockbead, which are typically used for ductile materials like mild steel, are shown in (a). The redesigned clamping dies for testing AZ31B sheet, with three small lockbeads using a 1.5 mm radius for each bead, are shown in (b). The original LDH tooling was obtained from Interlaken Corporation

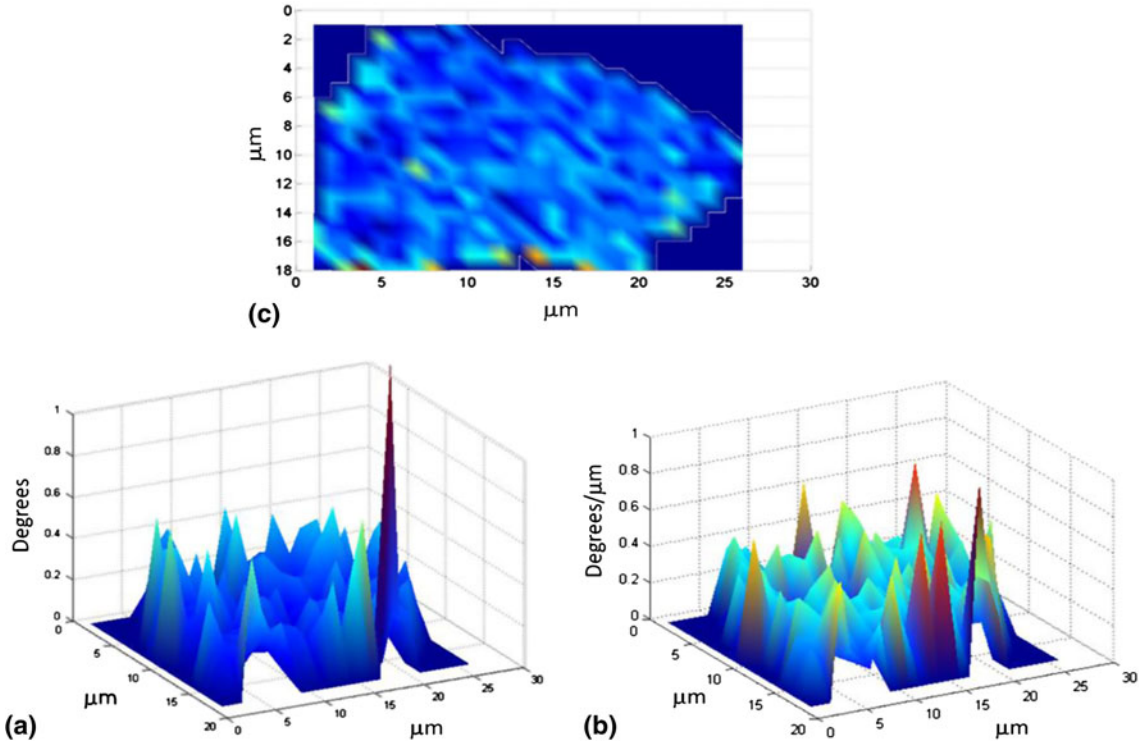

Fig. 4 Misorientation (on the *z*-axis, in degrees) across a grain from a chosen reference point in the center of the grain (a) and misorientation between neighboring points (proportional to lattice curvature) across the same grain for undeformed AZ31B Mg (b). A top view of the grain is shown in (c) with the misorientation from (a)

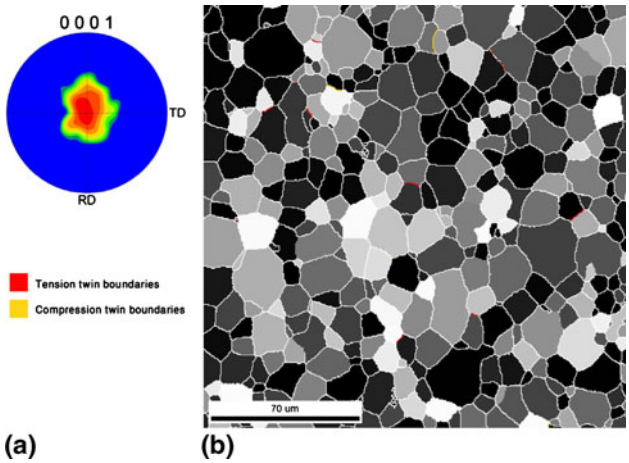

Fig. 5 (a) Pole figure showing strong basal texture and (b) microstructure of annealed AZ31B, with twin fraction of 0.011 and average grain size of 12 µm

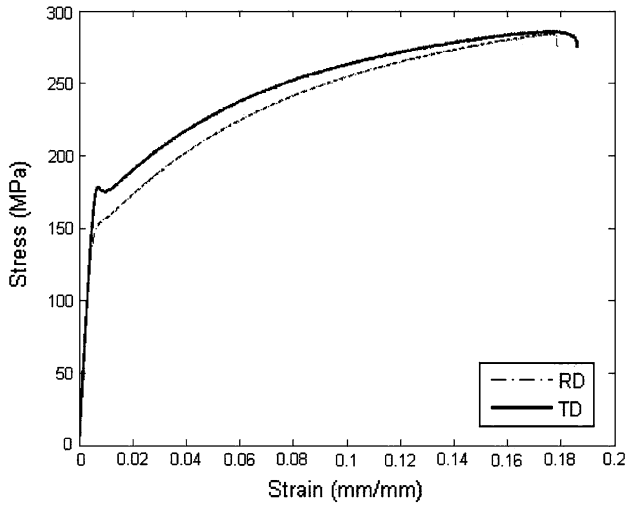

Fig. 6 Stress-strain plot of annealed AZ31B rolled sheet. Yield stress is greater when the sheet is strained along the TD vs. the RD

with the trace of the twinning plane, according to a method developed in prior work (Ref 12, 13). For magnesium, the tensile twin planes and directions are $\{1012\}\langle 1011\rangle$, while the compression twin planes and directions are $\{1011\}\langle 1012\rangle$. After identification of the length of the twin boundaries within the scanned region (200×200 µm), the twin fraction was computed as the total length of the twin boundaries by the length of all boundaries having misorientation $>10°$.

3.2 Calculation of Dislocation Density

Using recently developed high-resolution EBSD techniques (Ref 14, 15), EBSD patterns may be used to extract detailed information regarding the local elastic strain of the crystal lattice, as well as high-resolution lattice orientation data. From an analysis of the perturbation in orientation between neighboring points, the local lattice curvature may be determined

(in the plane of the sample surface), leading to the ability to map dislocation density across the scan. The dislocation density tensor captures the structure of geometrically necessary dislocations that perturb the lattice. It may be described by a second-rank tensor, with components α_{ij}, which give the line density of dislocations with Burgers vectors in the direction of x_j and lines extending in the direction of x_i. Nye originally defined this tensor using only the lattice curvature components, κ_{ij}, but later Kröner included the effect of the lattice strain in a form that can be expressed by the following representation (Ref 16, 17):

$$\alpha_{ki} = \kappa_{ki} - \delta_{ki}\kappa_{pp} + \in_{klj} \varepsilon^{e}_{ij,l} \quad \text{(Eq 1)}$$

where $\in_{klj}$ is the permutation tensor. Note that since lattice curvature information in the "3" direction is unavailable, only 5 of the 9 dislocation density tensor components can be resolved.

The main issue with applying this framework to the AZ31B samples relates to the quality of the EBSD images acquired. Compared to other easily polished metals, the image quality as determined by the EBSD software (Ref 18) is very low (the step size was 1 μm, and the angular accuracy is within 0.5° for this software, while the average measured misorientation across the grain is 0.686). Figure 4 illustrates the issue by plotting the misorientation across a single grain of the undeformed sheet, relative to a single point, as determined by the EBSD software. There is clearly a significant amount of noise in the measurements, and this is reflected in the local curvature calculations (also shown in Fig. 4). While the curvature, and hence related dislocation density, increases toward the edges of the grain as would be expected, the measured levels are only just above the noise levels of the method.

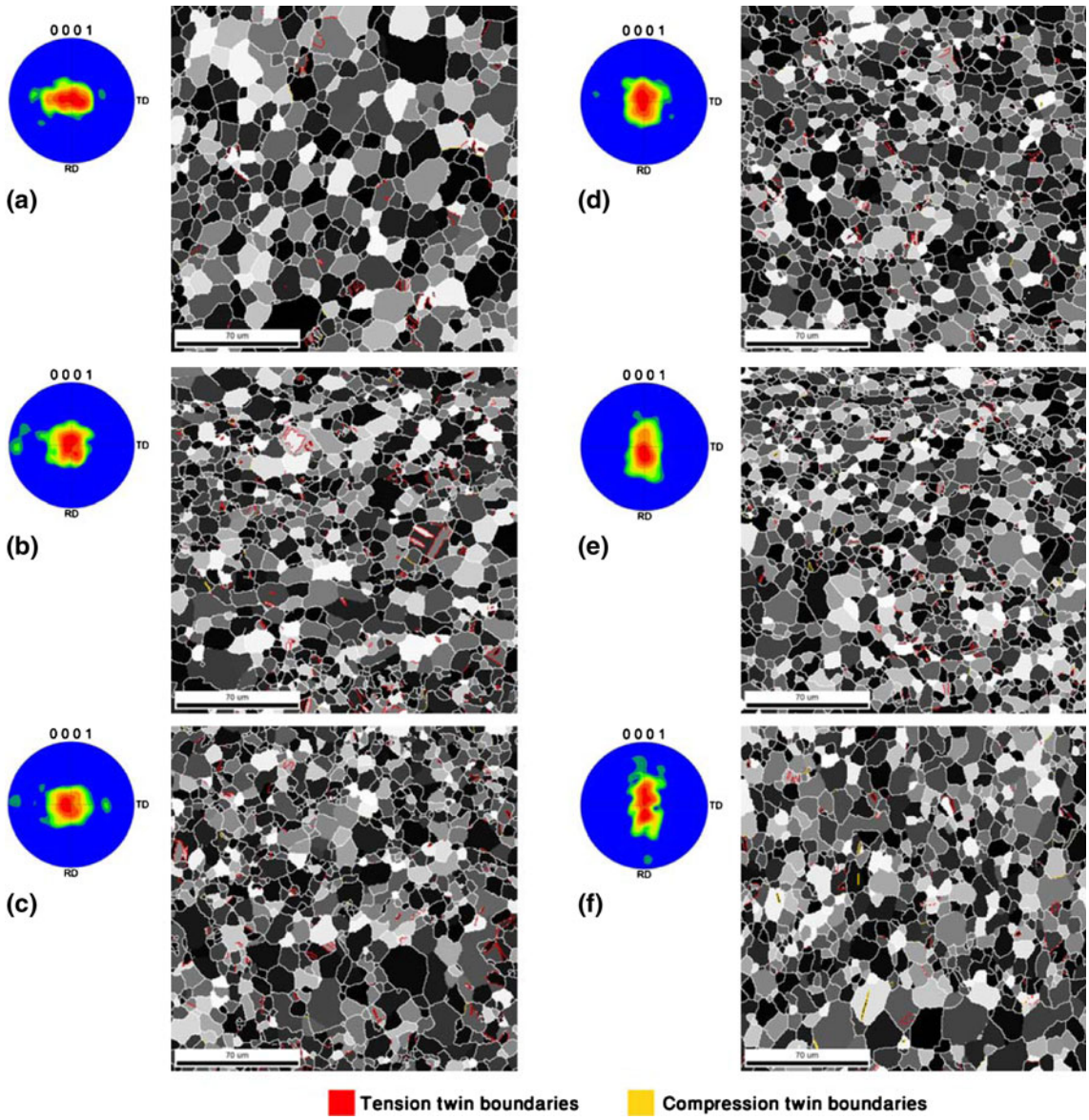

Fig. 7 Pole figures and microstructures for AZ31B Mg strained along the RD in uniaxial tension to a strain of (a) 4% with twin fraction of 0.045, (b) 8% with twin fraction of 0.052, and (c) 12% with twin fraction of 0.033. Pole figures and microstructures for AZ31B Mg strained along the TD in uniaxial tension to a strain of (d) 4% with twin fraction of 0.013, (e) 8% with twin fraction of 0.009, and (f) 12% with twin fraction of 0.007

However, when the noise levels are analyzed the dislocation structure can be resolved in a strained sample and this information can provide direction on defect nucleation and failure, as will be shown in the results section below.

4. Results and Discussion

Prior to analysis of strained specimens the texture and twin fractions were computed in the annealed and undeformed AZ31B material. The 0001 pole figure and microstructure are shown in Fig. 5, where the calculated twin fraction was 0.011 and the average grain size was 12 μm.

The AZ31B sheet has a strong basal texture in the annealed condition and is relatively free of twins, which is in agreement with prior work on this material (Ref 19, 20). With the basal poles oriented substantially normal to the plane of the sheet, basal slip is favored when the sheet is strained in uniaxial tension. However, the orientation of the sheet has an influence on the yield stress, where a specimen with major strain axis oriented along the RD had a lower yield stress than a specimen oriented along the TD. This is explained by the spreading of the basal poles along the RD of the sheet, as seen in Fig. 5a, which

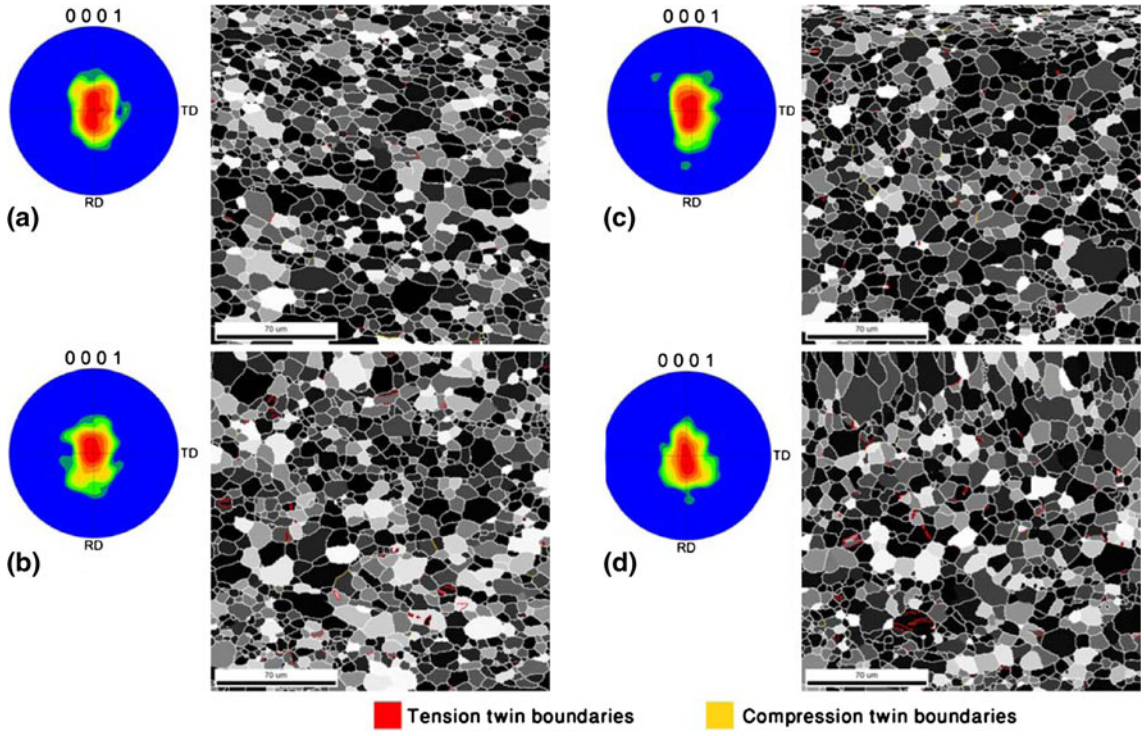

Fig. 8 Pole figures and microstructures for AZ31B Mg strained in biaxial tension and then scanned by EBSD along the RD direction: (a) 4% effective strain with twin fraction of 0.001 and (b) 8% effective strain with twin fraction of 0.017. Pole figures and microstructures for AZ31B Mg strained in biaxial tension and then scanned by EBSD along the TD direction: (c) 4% effective strain with twin fraction of 0.004 and (d) 8% effective strain with twin fraction of 0.011

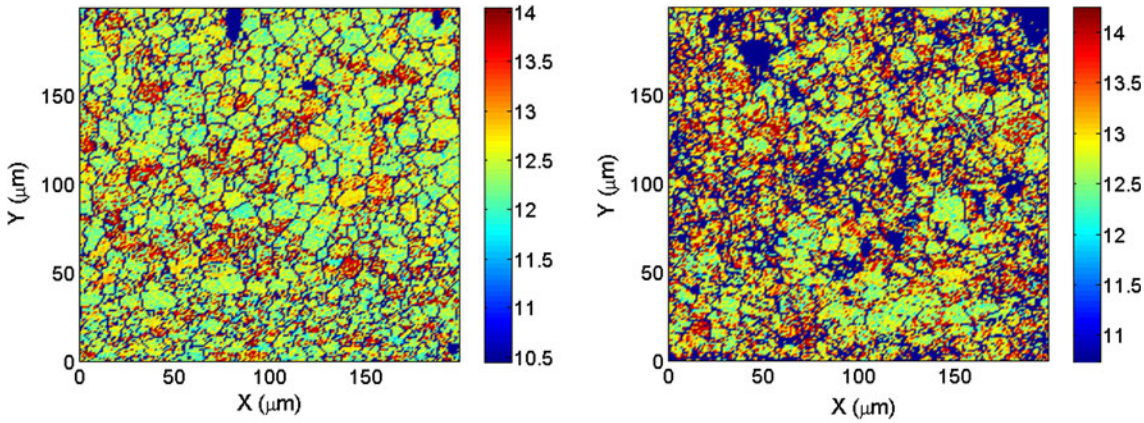

Fig. 9 Dislocation density maps for undeformed (left) and 8% tensile strain sample (right). The maps are for the norm of the dislocation density tensor. The color bar scale indicates the natural log of the dislocation density. Dark regions indicate points of poor quality images

makes it easier to activate basal slip when the sheet is pulled in tension along the RD (Ref 20, 21). This was seen in uniaxial tension testing done in the current work, with initial strain rate of 4.4×10^{-4} s^{-1}. The yield strengths were calculated as an average of three specimens in each direction. For the RD, yield strength was 150.5 MPa, while for the TD the yield was 178.2 MPa. Typical stress-strain curves are shown in Fig. 6.

Tension testing was done for specimens in both the RD and TD directions for strains of 4, 8, and 12%. After tension testing to prescribed strain levels EBSD scans were done on each specimen, as previously described in Fig. 1, and textures and twin fractions were computed. The pole figures, microstructures, and corresponding twin fractions are shown in Fig. 7.

The textures of the AZ31B sheet do not show much change as a function of strain, with a strong basal texture persisting in both the RD and TD specimens, although tightening of the texture is seen in the specimens pulled along the RD as the material achieves a stable orientation. Compared to the annealed material the strained specimens have greater twin fractions, although the increase in twin fraction is not substantial and does not occur in a straight line. Twin fraction as a function of strain is shown in Fig. 8 for uniaxial and biaxial tension experiments.

Both the RD and TD specimens with 12% strain had computed twin fractions which were about the same or less than those of the 4 and 8% specimens. While it is expected that twin density would increase with greater levels of strain, it is possible that deformation has altered the twin boundaries, making it more difficult to distinguish between a normal boundary and a twin boundary. It has also been shown in prior studies that uniaxial tension does not result in substantial twinning in AZ31B sheet material, especially when the grain size is fine (Ref 21, 22). The sheets used for the current work had an average grain size of 12 μm. Given the low level of twinning it is also not surprising to see relatively small changes in texture with increasing levels of strain.

In addition to uniaxial tension some biaxial tension experiments were done, where sheets of AZ31B were strained to 4 and 8% effective strain. The pole figures, microstructures, and corresponding twin fractions are shown in Fig. 8.

Surface strains on the biaxial specimen were about 2 and 4%, which correspond to effective strains of about 4 and 8%. The textures in these specimens have also not changed much with increasing strain, while the twin fractions are lower than was seen in uniaxial tension specimens for the same equivalent strain level.

Based on these observations it appears that twin fraction may not be a strong indicator, or precursor, of failure for AZ31B when the sheet has a strong basal texture and fine-grain size, and when strains are uniaxial tension or biaxial tension. In this case dislocation density may be a better indication of failure location, especially in the sheets used for this study, where basal slip is favored based on the texture of the sheet and the mode of deformation.

The measurement of dislocation density depends on the noise level in the data obtained by an EBSD scan. For example, when a sample of the AZ31B sheet is strained to 8% in uniaxial tension the dislocation density is only measured to be

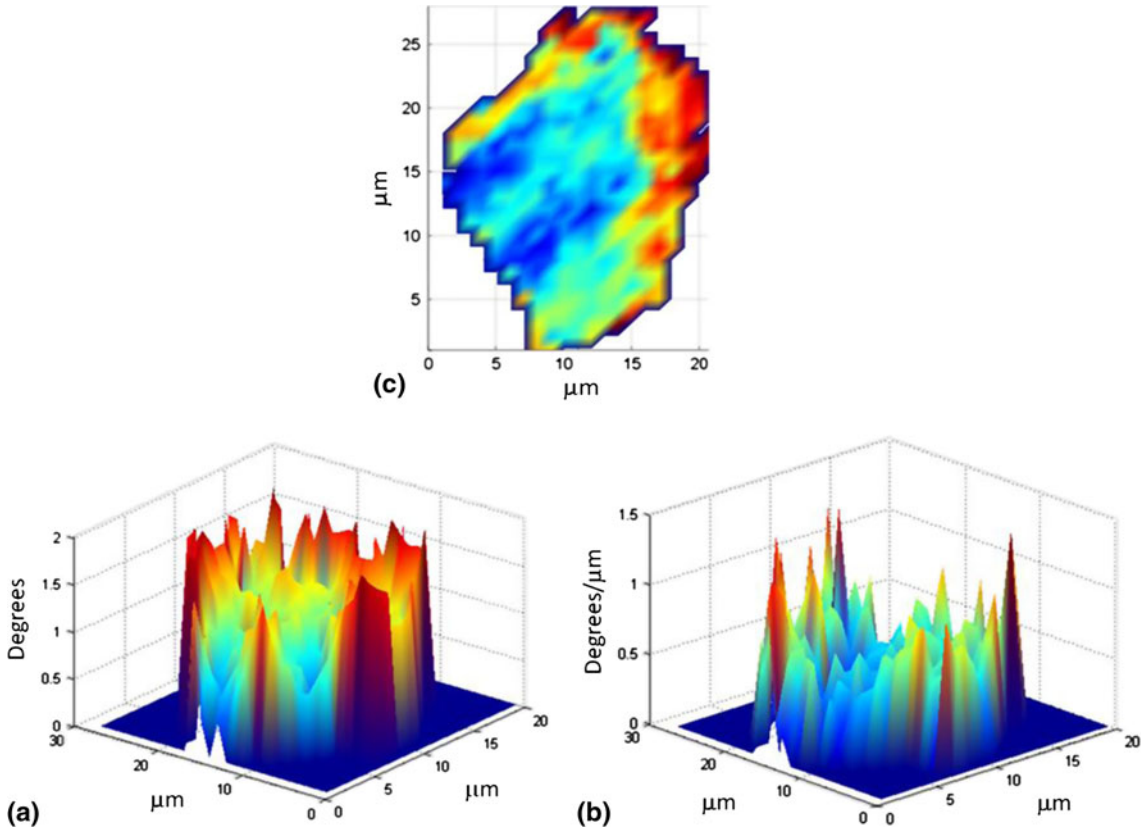

Fig. 10 Misorientation (on the *z*-axis, in degrees), (a) across a grain from a chosen reference point in the center of the grain and (b) misorientation between neighboring points (proportional to lattice curvature) across the same grain for 8% tensile strained AZ31B. A top view of the grain is shown (c) with the misorientation from (a)

marginally higher than the undeformed sample, as shown in Fig. 9.

However, when the noise levels are analyzed it appears that the dislocation structure is now rising significantly above the noise level, as seen in Fig. 10.

The average dislocation density for the undeformed sample is measured at 1.2×10^{13}, while for the deformed sample the value is 2.8×10^{13}. Hence, the resolution for dislocation density measurements using the current polishing method is approximately 2×10^{13}. It should be noted that the effect of being able to resolve only 5 of the 9 dislocation tensor values would affect the overall dislocation density calculation by approximately a factor of 2, although this point is still a subject of ongoing research (Ref 23).

Methods of improving the sample preparation are being investigated by the authors in an effort to improve the dislocation density resolution. However, even at current resolution limits, the dislocation density data is expected to produce vital information regarding the local dislocation structure, and potential defect nucleation sites, for highly deformed samples.

5. Summary and Conclusions

EBSD scans were used to study twin fraction as a function of strain level and strain state in annealed AZ31B magnesium alloy sheets. For uniaxial tension, twin fractions rose modestly as applied strain increased to 8%, but then for the specimen with 12% strain the twin fraction fell back to the same level or less than that of the specimen with 8% strain. The initial strong basal texture was little changed over the range of strains imposed, although the texture did tightened with strain along the RD as the material achieved a stable orientation. Biaxial tension experiments were carried out to levels of 4 and 8% strain, showing lower levels of twin fraction for the same equivalent strain compared to uniaxial tension specimens. In contrast to twin fraction, dislocation density in a uniaxial tension specimen strained to 8% was shown to be significantly higher than that of an annealed specimen. Therefore, dislocation density may be a better indicator of failure location for annealed AZ31B sheets strained in tension. Future work will focus on using both twin fraction and dislocation density as indications of potential failure in AZ31B sheet subjected to complex strain paths and to various forming temperatures.

Acknowledgments

This work was funded by NSF grant CMMI-0928923. AZ31B sheet materials were provided by General Motors Research Labs.

References

1. S. Das, Primary Magnesium Production Costs for Automotive Applications, *J. Met.*, 2008, **60**, p 63–69
2. H. Li, E. Hsu, J. Szpunar, R. Verma, and J.T. Carter, Determination of Active Slip/Twinning Modes in AZ31Mg Alloy Near Room Temperature, *J. Mater. Eng. Perform.*, 2007, **16**, p 321–326
3. S. Lee, Y.-H. Chen, and J.-Y. Wang, Isothermal Sheet Formability of Magnesium Alloy AZ31 and AZ61, *J. Mater. Process. Technol.*, 2002, **124**, p 19–24
4. F.-K. Chen and T.-B. Huang, Formability of Stamping Magnesium-Alloy AZ31 Sheets, *J. Mater. Process. Technol.*, 2003, **142**, p 643–647
5. B.L. Mordike and T. Ebert, Magnesium: Properties—Applications—Potential, *Mater. Sci. Eng. A*, 2001, **302**, p 37–45
6. F.H. Froes, D. Eliezer, and E. Aghion, The Science, Technology, and Applications of Magnesium, *J. Met.*, 1998, **50**(9), p 30
7. Forming of Magnesium Alloys. ASM Handbook, Vol 14B, p 625
8. E. Doege and G. Kurz, Development of a Formulation to Describe the Work Softening Behavior of Magnesium Sheets for Heated Deep Drawing Processes, *CIRP Ann. Manuf. Technol.*, 2001, **50**, p 177–180
9. J. Koike, Enhanced Deformation Mechanisms by Anisotropic Plasticity in Polycrystalline Magnesium Alloys at Room Temperature, *Metall. Mater. Trans. A*, 2005, **36**, p 1689–1696
10. E. Doege and K. Dröder, Sheet Metal Forming of Magnesium Wrought Alloys—Formability and Process Technology, *J. Mater. Process. Technol.*, 2001, **115**, p 14–19
11. EDAX TSL OIM™ 6.0 software, Draper, UT 84020
12. V. Randle, A Methodology for Grain Boundary Plane Assessment by Single-Section Trace Analysis, *Scr. Mater.*, 2001, **44**, p 2794–2798
13. S.I. Wright and R.J. Larsen, Extracting Twins From Orientation Imaging Microscopy Scan Data, *J. Microsc.*, 2002, **205**(3), p 245–252
14. A.J. Wilkinson, G. Meaden, and D.J. Dingley, High-Resolution Elastic Strain Measurement From Electron Backscatter Diffraction Patterns: New Levels of Sensitivity, *Ultramicroscopy*, 2006, **106**, p 307–313
15. J. Kacher et al., Bragg's Law Diffraction Simulations for Electron Backscatter Diffraction Analysis, *Ultramicroscopy*, 2009, **109**(9), p 1148–1156
16. E. Kroner, *Physics of Defects*, R. Balian, Ed., North-Holland, Amsterdam, 1981, p 219–315
17. C.D. Landon, B. Adams, and J. Kacher, High Resolution Methods for Characterizing Mesoscale Dislocation Structures, *J. Eng. Mater. Technol.*, 2008, **130**(2), p 021004–021008
18. S.I. Wright and M.M. Nowell, EBSD Image Quality Mapping, *Microsc. Microanal.*, 2006, **12**, p 72–84
19. A. Jain and S.R. Agnew, Modeling the Temperature Dependent Effect of Twinning on the Behavior of Magnesium Alloy AZ31B Sheet, *Mater. Sci. Eng. A*, 2007, **462**, p 29–36
20. G. Proust, C.N. Tome, A. Jain, and S.R. Agnew, Modeling the Effect of Twinning and Detwinning During Strain-Path Changes of Magnesium Alloy AZ31, *Int. J. Plast.*, 2009, **25**, p 861–880
21. X.Y. Lou, M. Li, R.K. Boger, S.R. Agnew, and R.H. Wagoner, Hardening Evolution of AZ31B Mg Sheet, *Int. J. Plast.*, 2007, **23**, p 44–86
22. R.H. Wagoner, X.Y. Lou, M. Li, and S.R. Agnew, Forming Behavior of Magnesium Sheet, *J. Mater. Process. Technol.*, 2006, **177**, p 483–485
23. W. Pantleon, Resolving the Geometrically Necessary Dislocation Content by Conventional Electron Backscattering Diffraction, *Scr. Mater.*, 2008, **58**, p 994–997